

RECEPTOR-MEDIATED ENDOCYTOSIS MODELING OF ANTIBODY-DRUG CONJUGATES TO THE RELEASED PAYLOAD WITHIN THE INTRACELLULAR SPACE CONSIDERING TARGET ANTIGEN EXPRESSION LEVELS*

Jong Hyuk Byun¹, Anna Park¹ and Il Hyo Jung^{1,†}

Abstract An antibody-drug conjugate (ADC) is one of the effective treatment modalities designed as a targeted therapy for treating tumors. Certain ADCs such as brentuximab vedotin are known to kill negative tumor cells indirectly via membrane permeability and bystander-killing effect and to kill positive tumor cells directly. In this study, we propose a mathematical model to describe the ADC-receptor endocytosis mechanism and to predict payloads over a time profile more accurately, while considering target antigen-positive (Ag+)/negative (Ag-) cells. We discuss how the target-antigen expression levels derived using a ratio of Ag+ to Ag- cells determine the payload release in the intracellular space. The model is aimed at capturing the amount of the payloads based on the target expression levels with the total number of cells fixed. The results indicate that (i) the profile of the total payloads over a time within the intracellular space is less influenced by the target expression levels after a time period, but the slope at the growth phase in which the payload increases is determined by the target expression levels, (ii) the change in the area under the curve of the total intracellularly released payload with a change in the ratio of Ag+ to Ag- cells is more significant due to the initial ADC injection, (iii) the fluctuations in the released payloads within the Ag+ cells increase as the target expression levels decrease, unlike in the case of Ag- cells or extracellular space. In addition, the time t_{max} that corresponds to the maximum payload concentration C_{max} is shifted towards the right as the target-antigen levels decrease, and it is strengthened by an increase in the initial free ADCs. The proposed model may reduce the discrepancy between the experiment and the model in the prediction of payloads over time profile.

Keywords Antibody-drug conjugates (ADCs), ADC mathematical model, bystander-killing effect, target antigen expression level, drug delivery, receptor-mediated endocytosis.

MSC(2010) 92B05, 74L15, 92C40.

[†]The corresponding author. Email address:ilhjung@pusan.ac.kr(I. H. Jung)

¹Department of Mathematics, Pusan National University, Busan, 46241, South Korea

*This work was supported by the National Research Foundation of Korea (NRF) grant funded by the Korea government (MSIT) (NRF-2020R1C1C1A01004631 and NRF-2019R1A2C2007249).

1. Introduction

Antibody drug conjugates (ADCs) are complex engineered compounds that link monoclonal antibodies (mAbs) to payloads [15,24,26]. mAbs are responsible for targeting a specific antigen on the surface of the tumor cells. For example, trastuzumab binds to the human epidermal growth factor receptor 2 (Her2) antigen that is commonly expressed in the tumor cells of breast cancer patients [27]. cAC10 binds to the CD30+ target antigen that is commonly expressed in Hodgkin's lymphoma and anaplastic cell lymphoma [35]. THIOMAB IgG1 and humanized recombinant IgG1k antibodies recognize *Staphylococcus aureus* and a unique epitope of human EGFR, respectively [8,23]. In addition, anti-TENB2 binds TENB2, a transmembrane proteoglycan protein, and attention has recently been focused on TENB2 as a promising target antigen owing to its overexpression in human prostate tumors and rapid internalization [5]. Cytotoxic payloads in the ADC complex are responsible for killing the tumor cells. Emtansine (DM1) and monomethyl auristatin E (MMAE) are cytotoxic payloads that prevent microtubule polymerization and are used to treat breast cancer and Hodgkin's lymphoma or anaplastic large cell lymphoma, respectively [26]. A rifamycin-class antibiotic (dmDNA31) via a protease-cleavable linker is used for first-line tuberculosis treatments [8]. The humanized Zt/g4 antibody binds to the receptoru-d'origine-nantais receptor tyrosine kinase, and this is conjugated with MMAE using a dipeptide linker for pancreatic cancer [37].

ADCs carry DM1 or MMAE into the cells through binding of mAbs to Ag+ antigens on the surface of the tumor cells. These ADCs are subsequently internalized through endocytosis. Payloads with cleavable linkers are commonly released because of lysosomal protease (brentuximab vedotin), pH, or glutathione sensitivities. However, the explosive activity of the payloads with non-cleavable linkers relies on the degradation of the total antibody, thus ultimately releasing an amino-acid-linker-cytotoxin construct [13]. Once released intracellularly, these payloads bind to tubulin and inhibit microtubule polymerization, which leads to cell death. mAbs, linker, and payloads perform critical roles in defining the target specificity, the stability of the complex, and mechanism of cytotoxic activity, respectively. In vivo stability and efficacy of ADCs can be improved by optimizing linkers and by selecting appropriate antibodies and payloads [2,3].

T-DM1 and depatuxizumab mafodotin are not known to diffuse into neighboring cells because of non-cleavable linkers, that is, no bystander-killing effects are observed, but brentuximab vedotin or anti-TENB2-MMAE are known to kill adjacent tumor cells that do not express the target [3,5,8,23]. These ADCs are quite potent, and the payload release occurs in lysosomes [7]. A cell-level systems Pharmacokinetic-Pharmacodynamic (PK-PD) model is developed to characterize the bystander effect of Trastuzumab-vc-MMAE using experimental data; in addition, two cell-level PK models are integrated, and the model thus obtained captures the observed data well, as demonstrated in [30]. Okeley et al. [25] reported an antigen-independent cytotoxic effect on CD30-negative cells that is likely caused by MMAE released from cocultured CD30-positive cells. The bystander-killing effect does not depend only on internalization [32] and [31]. The extent of the bystander killing of Ag- cells is investigated in [19]. In this work, the biophysical properties and the amounts of the released payloads were established as the main factors that determine the overall ADC potency and bystander killing in vitro and in vivo.

Some models [16,29,34] are introduced to describe the ADC mechanism. In [29],

the application of the single cell ADC PK-PD model is explored in an in-vivo system PK-PD framework, where the occupancy to tubulin by MMAE was used to drive the killing of tumor cells. Furthermore, both the models presented in [16,34] demonstrated ADC pathways for tumor penetration from receptor-mediated endocytosis to payload release, and they explored the tumor-growth inhibition due to the released payload according to the number of targets and drug antibody ratio (DAR), respectively. However, the change in the payload according to the target positive/negative (Ag+/Ag-) cells was not taken into consideration, although they discussed the factors affecting the ADC efficacy.

In this study, a mathematical model is developed to predict the change in the amount of the released payloads due to a change in the ratio of Ag+ to Ag- cells, with the total number of Ag+/Ag- cells fixed (See Fig.1). Assuming that the amount of target-antigen expression level in each Ag+ cell is the same, the number of Ag+ cells is determined by varying the target-antigen expression levels that are governed by a fraction number $\beta \in (0, 1]$. This implies that β and the number of Ag+ cells are proportional. In addition, the changes in membrane permeability [19, 33] that mediates the bystander-killing effect on the amount of intracellular payload release shall also be explored, together with the changes in Ag+/Ag- cells. The results are summarized as follows. The time profile of the total payloads (payloads within the sum of Ag+ and Ag- cells) in the intracellular space is less influenced by the Ag+/Ag- ratio after the time phase in which the payload grows, but the slope at the time phase in which the payload grows is determined based on the target-antigen expression level. In addition, t_{max} is shifted towards the right as β decreases, and it is strengthened by the initial free ADC administration. The change in the area under the curve (AUC) of the total intracellularly released payload depending on β is strengthened by the initial ADC administration. The released payloads in the Ag+ cells demonstrate a greater fluctuation as the number of Ag+ cells reduces, in contrast to the payloads in the Ag- cells or in the extracellular space. We opine that the predicted amount of the payloads in the model may be biased if we do not take into consideration about dividing the cells. This could result in an over- or under-estimation of the parameter values even if the data fitting in the model is good. Therefore, the proposed model may reduce the discrepancy of prediction of the payload over time profile between the experiment and the model. Improvements in the ADC design are still desirable owing to the narrow therapeutic window of these compounds despite some clinical success with ADCs in patients with solid tumors and hematological malignancies [20]. This model could provide a clue for successful clinical translation of ADCs.

To support the obtained results, we first present the assumptions before the model presentation. The model appears to be similar to previously existing models, but it is different in terms of the target and payload by the ratio of the cells. We additionally apply Ag+/Ag- cells in the model for the endocytosis process as well as for the payload release. The robustness of the model is verified through mathematical analysis. The target-antigen expression levels are then investigated to understand why we divide the whole cells into Ag+/Ag- cells.

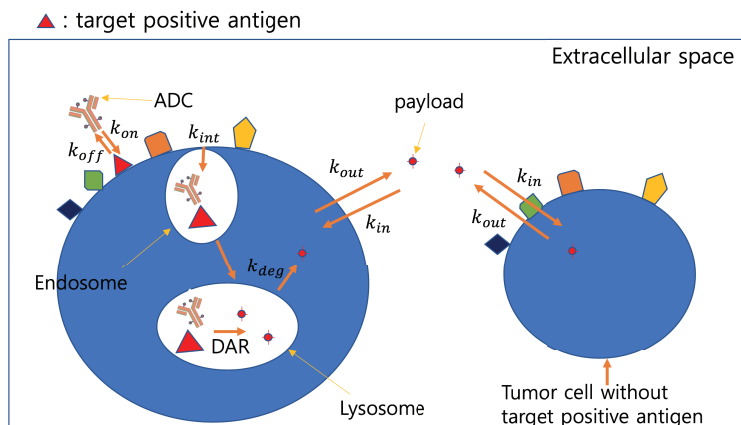


Figure 1. Mechanism of action of ADCs. After ADCs bind to the target antigens, the ADC-target complex undergoes internalization (endocytosis) and is subsequently degraded by lysosomes. Some of the intracellular release payloads in the cytosol permeate into the extracellular spaces and then enter into the cytosol of neighboring tumor cells. Some neighboring cells are Ag- cells that are subject to bystander killing. A specific target antigen is indicated by a red triangle.

2. Material and methods

Assumptions

Before presenting the model, our assumptions are presented as follows:

- The in vitro model is constructed such that the elimination rates of the free ADCs and the released payloads are ignored. In addition, the in vitro assumption facilitates the simplification of the model such that the delivery processes of the ADCs from the blood administration to the tumor cells are not considered.
- The synthesis rate of the free target antigen is of the zeroth-order. This assumption has been considered in many studies.
- The internalized rate of bounded ADCs and the degradation rate of the free target antigens are identical. Thus, the total target (free target + bounded ADCs) is constant.
- The free ADCs cannot release the payloads via phagocytes or other mechanisms without the internalization process. That is, the payload release occurs only by endocytosis and subsequent lysosome trafficking.

The above assumptions are commonly used to describe the ADC-target antigen binding process [1, 10, 22]. The following assumption is regarding the binding fraction. The ideas are followed by [11, 16, 18, 34].

- ϵ is used to take into consideration the fraction of free ADCs that bind with the target antigen. ϵ_p is also used to account for the fraction of the payload when the extracellular payload is diffused into the intracellular space.

The following assumptions are only considered for the model we use hereafter. This is related to the endocytosis process and the Ag⁺/Ag⁻ cell division.

- On assuming a mean retention time of $1/k_{deg}$ from internalization, endosome, late endosome, and lysosomes of the bounded ADC to the payload release, an exponential distribution can be considered in the model. This simplifies the model, although the robustness of the data fitted from the experiments is slightly reduced, and the physical meaning of the processes is lost.
- The number of total cells consisting of Ag⁺/Ag⁻ is constant.
- The concentration of the target antigen in each Ag⁺ cell is the same. Thus, the total number of antigens in the entire system varies with the fraction of Ag⁺ and Ag⁻ cells.
- There exists $\beta \in (0, 1]$, such that the ratio of Ag⁺/Ag⁻ cells is determined by β .
- The binding process of the microtubule and intracellularly released payload are not taken into consideration.

We discuss β in greater detail in the next section. To develop an in vitro ADC model, the average DAR, which is the number of payloads over a mAb, is known as 4, as shown in [36], although it is important to define the DAR, which influences the ADC efficacy [12]. All the model compartment units are assigned a concentration, nM , after the translation of amount/volume through the compartment. Tissue transport is governed by diffusion, and some authors [16, 34] have used the Krogh cylinder model to account for tissue transport. These models considered radial drug transport under an assumption of axisymmetric drug penetration and without convective forces. However, the focus of the present analysis is not the radius from the capillary to the tumor tissue; hence, this issue has been ignored. The intracellularly released payloads in the Ag⁺/Ag⁻ cells and the payloads within the extracellular space are considered to capture the bystander-killing effects and membrane permeability.

Determination of Ag⁺ cells based on target-antigen expression level

The expression level of the target antigen in the Ag⁺ cells determines the speed of the binding process of the ADCs. If the target-antigen level is higher, then the ADC–target binding is faster, thus resulting in quick ADC deposition. Let β be a fraction number in $(0, 1]$ that is used to describe the expression level of the target antigen. $\beta = 0$ indicates no target cells (no Ag⁺ cells), and this need not be discussed because receptor-mediated endocytosis does not occur. $\beta = 1$ indicates that all the cells consist of Ag⁺ cells. Because the total number of cells is fixed, the ratio of Ag⁺/Ag⁻ cells changes according to the value of β . Therefore, if the initial free target concentration of βR_0 and $\beta = 1$, then the cells comprise Ag⁺ cells only. If the number of Ag⁺ cells is decreased as the value of β is reduced, then the number of Ag⁻ cells increases as the Ag⁺ cells decrease. In applications, it is impossible to divide the two types of cells exactly because the cell structure is

heterogeneous. However, we opine that the concept of dividing cells based on their concentration may aid in understanding the phenomenon accurately with respect to the goodness of fit of the model and the experiments rather than one type of cell. Let the initial target concentration be $R_0 = 833nM$, as shown in [16]. Then β determines the target concentration on the surface of the Ag+ cells. We assume that the maximum initial concentration of the target antigen is $R_0 = 833nM$, such that $\beta = 1$ in this case. The values of β can then be determined based on the fixed R_0 .

2.1. Modeling to ADC receptor-mediated endocytosis and payload release

In the ADC-target binding process, we denote ADCs (C_{adc}), target antigens (R), and ADC-target complex (bounded ADC, B_{adc}). Let the ADC association and dissociation rates be k_{on} and k_{off} , respectively, which reflect the relationship $k_{off} = k_{on} \cdot k_D$, where k_D is the dissociation constant.

$$\frac{dC_{adc}}{dt} = -k_{on} \frac{C_{adc}}{\epsilon} \cdot \beta R + k_{off} B_{adc}. \tag{2.1}$$

The ADCs bind to R reversibly, thus forming a bound complex. Let k_{syn} be the zero-order target recycle rate and k_{int} be the first-order ADC-target internalization rate. Thus, the target dynamics is considered as follows.

$$\frac{d(\beta R)}{dt} = \beta k_{syn} - k_{int}(\beta R) - k_{on} \frac{C_{adc}}{\epsilon} \cdot \beta R + k_{off} B_{adc}. \tag{2.2}$$

If $\beta = 1$, then the initial value R_0 of R can be defined as follows. $R_0 = k_{syn}/k_{int}$ from $dR/dt = 0$ and $C_{adc} = 0$. This equation is different from that considered in many studies [1, 10, 21] because the model takes into consideration the target-antigen expression level β . Let k_{int} be the ADC-target internalization rate, which reflects the endocytosis of the bounded ADCs B_{adc} . The equation of the bounded ADCs including a binding fraction ϵ as explained above is then given by

$$\frac{dB_{adc}}{dt} = k_{on} \frac{C_{adc}}{\epsilon} \cdot \beta R - (k_{off} + k_{int}) B_{adc}. \tag{2.3}$$

It should be noted that the total target $\beta R + B_{adc}$ is constant because of the internalization rate k_{int} . This constant can be calculated because

$$\frac{d(\beta R + B_{adc})}{dt} = \beta k_{syn} - k_{int}(\beta R + B_{adc}),$$

and the result is as follows.

$$\beta R + B_{adc} = \frac{\beta k_{syn}}{k_{int}} + e^{-\frac{k_{int}}{\beta} t} \left(\beta R_0 - \frac{\beta k_{syn}}{k_{int}} \right) = \beta R_0,$$

because $R_0 = k_{syn}/k_{int}$. For each β , the concentration of the total target is always constant. Let βR and βR_0 be \tilde{R} and \tilde{R}_0 , respectively. The ADC-target binding model from Eqs. (2.1), (2.2), (2.3) follows as

$$\frac{dC_{adc}}{dt} = -k_{on} \frac{C_{adc}}{\epsilon} \cdot \tilde{R} + k_{off} B_{adc},$$

$$\begin{aligned}\frac{d\tilde{R}}{dt} &= \beta k_{syn} - k_{int}\tilde{R} - k_{on}\frac{C_{adc}}{\epsilon} \cdot \tilde{R} + k_{off}B_{adc}, \\ \frac{dB_{adc}}{dt} &= k_{on}\frac{C_{adc}}{\epsilon} \cdot \tilde{R} - (k_{off} + k_{int})B_{adc}.\end{aligned}\quad (2.4)$$

To describe the endocytosis process of the bounded ADCs within the intracellular spaces, we assume that the mean retention time of the endocytosis is $1/k_{deg}$, which implies an exponential distribution. This means that the process is given by one compartment. Here, the mean retention time is the time elapsed from the internalization to the payload release. Thus, bounded ADCs are separated into mAbs and the payloads within lysosomes. Let $C_{int,adc}$ be the bounded ADCs during the endocytosis phases. Then,

$$\frac{dC_{int,adc}}{dt} = k_{int}B_{adc} - k_{deg}C_{int,adc}.\quad (2.5)$$

The intracellular payloads are released after the last endocytosis phase. The released payloads in the cytosol are the result of the lysosomal degradation of the ADC [9]. Some intracellular released payloads permeate into the extracellular space through the tumor cell membranes, and the diffusion of the payload from this space (e.g., MMAE) into the neighboring cells may then trigger the bystander-killing effect. The extracellular payloads could penetrate into the cytosol at the rate of k_{in} and diffuse into the tumor interstitial space at the rate of k_{out} . For the bystander-killing effect, the released payloads $C_{int,p}$ within Ag+ cells and $C_{int,n}$ within Ag- cells are considered. For a fixed total tumor size depending on β , the ratio of the Ag+ and Ag- tumor cells are determined, and the extent of bystander killing is explored. We define a constant α that represents a fraction of the payloads within lysosomes such that $\alpha \leq k_{deg}$, and this is because some of the ADCs fail to release payloads at the rate $(k_{deg} - \alpha)$ from $C_{int,adc}$. The ADCs are internalized in the lysosomes via endocytosis, which is followed by a degradation by lysosomal proteases. Based on [6] including a binding fraction ϵ_p as explained above, $C_{int,p}$, $C_{ext,p}$, and $C_{int,n}$ are given as follows.

$$\frac{dC_{int,p}}{dt} = \alpha \cdot DAR \cdot C_{int,adc} + \beta k_{in}\frac{C_{ext,p}}{\epsilon_p} - k_{out}C_{int,p},\quad (2.6)$$

$$\frac{dC_{ext,p}}{dt} = -k_{in}\frac{C_{ext,p}}{\epsilon_p} + k_{out}C_{int,p} + k_{out}C_{int,n},\quad (2.7)$$

$$\frac{dC_{int,n}}{dt} = (1 - \beta)k_{in}\frac{C_{ext,p}}{\epsilon_p} - k_{out}C_{int,n},\quad (2.8)$$

where $C_{ext,p}$ is the payload concentration within the extracellular space. It should be noted that all the time and concentrations units are in min and nM, respectively. Therefore, the receptor endocytosis model for deriving the payloads from the free ADCs is summarized as follows:

$$\begin{aligned}\frac{dC_{adc}}{dt} &= -k_{on}\frac{C_{adc}}{\epsilon} \cdot \tilde{R} + k_{off}B_{adc}, \\ \frac{d\tilde{R}}{dt} &= \beta k_{syn} - k_{int}\tilde{R} - k_{on}\frac{C_{adc}}{\epsilon} \cdot \tilde{R} + k_{off}B_{adc}, \\ \frac{dB_{adc}}{dt} &= k_{on}\frac{C_{adc}}{\epsilon} \cdot \tilde{R} - (k_{off} + k_{int})B_{adc},\end{aligned}$$

$$\begin{aligned}
 \frac{dC_{int,adc}}{dt} &= k_{int}B_{adc} - k_{deg}C_{int,adc}, \\
 \frac{dC_{int,p}}{dt} &= \alpha \cdot DAR \cdot C_{int,adc} + \beta k_{in} \frac{C_{ext,p}}{\epsilon_p} - k_{out}C_{int,p}, \\
 \frac{dC_{ext,p}}{dt} &= -k_{in} \frac{C_{ext,p}}{\epsilon_p} + k_{out}C_{int,p} + k_{out}C_{int,n}, \\
 \frac{dC_{int,n}}{dt} &= (1 - \beta)k_{in} \frac{C_{ext,p}}{\epsilon_p} - k_{out}C_{int,n},
 \end{aligned}
 \tag{2.9}$$

where $C_{adc}(0) = C_0$; $\tilde{R}(0) = \tilde{R}_0$; and $B_{adc}(0)$, $C_{int,adc}(0)$, $C_{int,p}(0)$, $C_{ext,p}(0)$, and $C_{int,n}(0)$ are zero.

3. Results

The simulation is implemented in MATLAB 2018b, MathWorks. The intrinsic function ODE45 in MATLAB is implemented for solving the system of ordinary differential equations. All the parameter values and initial values are presented in Table 1.

3.1. Mathematical analysis of model

3.1.1. Dynamics and equilibrium of payloads

The total released payload $C_{int,p} + C_{ext,p} + C_{int,n}$ does not depend on the value of β . To see this mathematically,

$$\frac{d(C_{int,p} + C_{ext,p} + C_{int,n})}{dt} = \alpha DAR \cdot C_{int,adc}.$$

If $C_{int,adc}$ is independent of β , then the total released payloads is also independent of β . Thus, from Eq. (2.5), the equation

$$(e^{k_{deg}t}C_{int,adc}(t))' = e^{k_{deg}t} \cdot k_{int}B_{adc}$$

can be solved using

$$C_{int,adc}(t) = k_{int}e^{-k_{deg}t} \int_0^t e^{k_{deg}s} B_{adc}(s) ds.$$

As $B_{adc} = \tilde{R}_0 - \tilde{R}$,

$$C_{int,adc}(t) = \frac{k_{int}}{k_{deg}}(1 - e^{-k_{deg}t})\tilde{R}_0 - k_{int}e^{-k_{deg}t} \int_0^t e^{k_{deg}s} \tilde{R}(s) ds.$$

Therefore, $C_{int,adc}$ is always non-negative owing to $R_0 \geq R$ and is independent of β . In addition, if $\tilde{R} \approx 0$, then

$$C_{int,adc} \approx \frac{k_{in}}{k_{deg}}(1 - e^{-k_{deg}t})\tilde{R}_0,$$

and if $\tilde{R} \approx \tilde{R}_0$, then $C_{int,adc} \approx 0$. These relationships indicate that if C_{adc} binds reversely to \tilde{R} , then $C_{int,adc}$ increases and then converges to zero as \tilde{R} returns to the baseline \tilde{R}_0 because C_{adc} decreases.

For the long-time behavior of each compartment, the model may eventually predict behaviors in how they conduct. To find an equilibrium point for the system (2.9), the rate of change was assumed to be zero. Then $\tilde{R}_0 = \beta k_{syn}/k_{int}$, which results in $B_{adc} = 0$, $C_{adc} = 0$, and $C_{int,adc} = 0$. From $d(C_{int,p} + C_{int,n} + C_{ext,p})/dt = \alpha \cdot DAR \cdot C_{int,adc}$, the total payloads are $C_{int,p} + C_{int,n} + C_{ext,p} = c$, where $C_{int,adc} \rightarrow 0$ as $t \rightarrow \infty$. From the system (2.6), $C_{int,p} = a \cdot \beta \cdot C_{ext,p}$, where

$$a = \frac{k_{in} \cdot \epsilon_p^{-1}}{k_{out}}, \quad (3.1)$$

we deduce the following.

$$\begin{aligned} C_{ext,p} &= \frac{\epsilon \cdot k_{out}}{k_{in}} (C_{int,p} + C_{int,n}) \\ &= \frac{1}{a} (C_{int,p} + C_{int,n}) \\ &= \frac{1}{a} (a\beta \cdot C_{ext,p} + C_{int,n}) \\ &= \beta \cdot C_{int,p} + \frac{1}{a} C_{int,n}, \end{aligned} \quad (3.2)$$

and thus, $C_{int,n} = a(1 - \beta)C_{ext,p}$. This results in

$$\begin{aligned} C_{ext,p} &= \frac{c}{a+1}, \\ C_{int,n} &= \frac{ca(1-\beta)}{a+1}, \\ C_{int,p} &= \frac{ac\beta}{a+1}. \end{aligned} \quad (3.3)$$

In addition, for the intracellular released payload,

$$C_{int,p} + C_{int,n} \rightarrow c \left(1 - \frac{1}{a+1}\right) \quad \text{as } t \rightarrow \infty.$$

In addition, under the initial administration C_0 , the amount of intracellularly released payloads is determined by k_{in} , k_{out} , and ϵ_p after a sufficient amount of time passes. It must be noted that c implicitly depends on β because $C_{int,adc}$ is determined by βR , followed by B_{adc} .

3.1.2. Dynamics of C_{adc} and B_{adc} , and system positiveness

C_{adc} declines slowly as the target antigen R is reduced. From Eq.(2.1), we have

$$\frac{dC_{adc}}{dt} = -\frac{k_{on}}{\epsilon} C_{adc} \cdot \beta R + k_{off}(\beta R_0 - \beta R),$$

where $B_{adc} = \beta R_0 - \beta R$. If $R \approx R_0$ (first and final phase), then the dynamics of C_{adc} decays exponentially with the rate parameter $\lambda = (k_{on}/\epsilon)\beta R_0$. From the summation of Eqs.(2.1) and (2.3) and the integration of the sum, we obtain

$$\begin{aligned} C_{adc} &= C_0 - \beta R_0 + \beta R(t) - k_{int}\beta R_0 \cdot t + k_{int} \int_0^t \beta R(s) ds \\ &= C_0 - \beta(R_0 - R(t)) - k_{int} \cdot t\beta(R_0 - R(\eta)), \end{aligned}$$

Table 1. Model parameter & initial values.

Parameter	Values	Unit	Description	Source
C_{adc}	10, 2.5, 0	mg/kg	initial concentration of ADCs	[16, 34]
R_0	833	nM	initial value of R	[16]
k_{on}	0.0426	$1/nM/min$	ADC association rate	[16]
k_D	0.5	nM	ADC dissociation constant	[16]
k_{syn}	1.65	nM/min	target recycle rate	[16]
k_{int}	k_{syn}/R_0	$1/min$	ADC-target internalization rate	[16]
ϵ	0.24	unitless	tumor void fraction	[16, 34]
k_{deg}	0.6912	$1/min$	ADC-target complex lysosomal degradation rate	[16]
DAR	4	unitless	drug antibody ratio	[14]
V_{adc}	2	ml/kg	distributed volume of ADCs	[34]
W	153	kg/mol	brentuximab-vedotin molecular weight	[36]
k_{in}	$8.46 \cdot 10^{-2}$	$1/min$	payload influx rate	[16]
k_{out}	$1.824 \cdot 10^{-3}$	$1/min$	payload efflux rate	[16]
ϵ_p	0.44	unitless	cell void fraction	[16]

where η is between 0 and t . It should be noted that the mean value theorem was used for the integral. This indicates that if $R(t) \approx 0$, that is, the binding process is under a quasi-steady state—assuming that the concentration of ADCs is much greater than that of R —then the dynamics of C_{adc} is bounded by linear functions because $0 \leq R(\eta) \leq R_0$.

We assumed that all the compartments are in $C^1(0, \infty)$, which is a set of continuously differentiable functions on $(0, \infty)$. We discuss that all the compartments are positive for $t > 0$. This analysis ensures that the model is mathematically well-posed [28] and is biologically realistic for representing the concentration of each compartment with no negative values. Firstly,

$$t_f = \inf\{t \in [0, \infty) : \tilde{R}(t_f) = 0\}. \tag{3.4}$$

Then, $dR/dt|_{t=t_f} = k_{syn} + (k_{off}/\beta)B_{adc} > 0$, which implies that $R(t_f - \epsilon) < 0$ for a sufficiently small ϵ . It is impossible to define t_f and $R_0 > 0$. As $R < R_0$ and $B_{adc} = \beta R_0 - \beta R$, $B_{adc} > 0$ for all the values of t . In a case wherein $C_{adc} = 0$ for some t , $dC_{adc}/dt = k_{off}B_{adc} > 0$. Thus, $C_{adc} \leq 0$ at $t - \epsilon$. As $C_0 > 0$, there is a t_u smaller than $t - \epsilon$ such that $C_{adc} = 0$. This result is also impossible for the defined t_f . If $C_{int,adc} < 0$ for some $t \in (0, \infty)$, then the rate of change of $C_{int,adc}$ is always positive, and we may assume that there is a t_p such that $C_{int,adc}(t_p) = 0$, where t_p is the infimum of t to be $C_{int,adc}(t) = 0$. As $B_{adc} > 0$ for all t , $dC_{int,adc}/dt > 0$ for $t > t_p$. It must also be noted that because $C_{int,adc}(0) = 0$, $C_{int,adc} > 0$ for $t > 0$. Other equations such as Eqs. (2.6), (2.7), and (2.8) can be easily proven.

3.2. Change in free ADCs and bounded ADCs according to β

As the amount of binding of \tilde{R} and C_{adc} decreases as β decreases (i.e., as β approaches zero), the amounts of Ag+ cells and the target antigens on the cells decrease. The free ADCs are then slowly disposing of, as shown in Fig.2. In addition, bi-exponential decay is observed, where rapid binding occurs by the amount of target antigen, and then decays slowly. The mean retention time of $C_{int,adc}$ also increases. This is because the rate at which the ADCs are bound depends on the time (assuming that the time to escape is constant) from the free ADC disposition; the smaller the value of β , the slower the binding speed of the free ADCs, thus

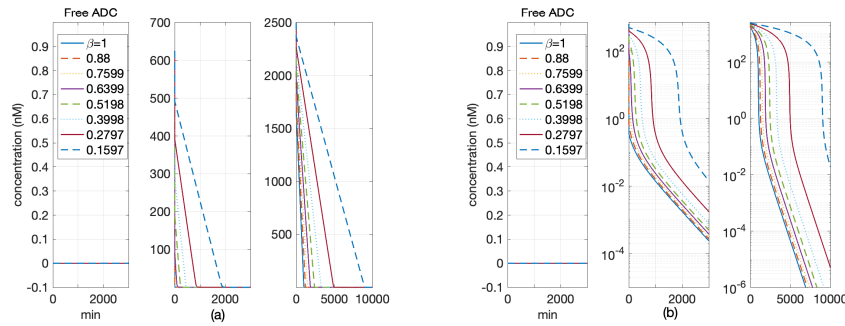


Figure 2. (a) Control ($C_0 = 0$) on the left panel and ADC administration of 2.5 mg/kg and 10 mg/kg at the center and right, respectively. As the value of β is small, the free ADC disposition occurs slowly. We assume that the ADC disposition occurs only through the endocytosis mechanism. (b) Log-scale along the Y-axis is used to present the initial dynamics.

resulting in the slow accumulation of $C_{int,adc}$. This affects the creation time of the bounded ADCs and $C_{int,adc}$ as well.

3.3. Relation between Ag+ expression levels and released payloads within the cells

The greater the value of β , the greater is the slope of $C_{int,p}$ in the time phase during which the payload increases and the equilibrium points, as shown in Fig.3. This is because the number of Ag+ cells is proportional to the value of β . Interestingly, the peak concentration C_{max} in $C_{int,p}$ in the time profile and the corresponding time t_{max} are shifted to the right as the value of β decreases. Furthermore, the fluctuation in C_{max} and the equilibrium values gradually increase as β decreases. This is because there is a time phase during which the slope temporarily becomes negative as $C_{int,p}$ increases when β is less than 1, and $\alpha DAR \cdot C_{int,adc} + k_{in}C_{ext,p}/\epsilon_p \leq k_{out}C_{int,p}$. Thus, we attempt to vary α , but such a gap appears larger as $\alpha > 0$ increases. Therefore, we highlight that $C_{int,p}$ is generated first in the case of the released payload owing to endocytosis, and the value of $C_{int,p}$ then decreases owing to permeability. There appears to be a phase during which the slope becomes negative. As $C_{ext,p}$ increases, $C_{int,p}$ increases again owing to permeability until the slope becomes 0. This appears to be similar to the rebound in the concentration of the target antigens, as shown in [1], and this requires further study. T_{max} is shifted to the right as the concentration increases, and the relative difference between C_{max} and the equilibrium value (i.e., $(C_{max} - E)/E_{\beta=1}$) is greater, where E represents the equilibrium points, and $E_{\beta=1}$ is the equilibrium point at which $\beta = 1$. Therefore, if an appropriate time phase is not selected, then it may become possible to select a larger value than the equilibrium value, and thus, the amount of payload in the Ag+ cells could be unreliable. $C_{int,n}$ increases, as shown in Fig.4, until the equilibrium point and intracellularly released payload $C_{int,p} + C_{int,n}$ in Fig.5 as well. There is a change in the aforementioned rate of increase as β increases, but the equilibrium points do not change. This is because the equilibrium value is independent of β as determined mathematically.

The concentration of $C_{int,p}$ is determined by C_0 and the Ag+ expression level,

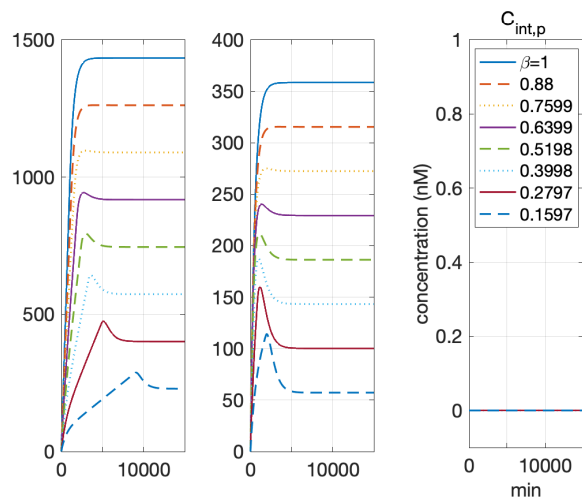


Figure 3. Control on the right panel and ADC administrations of 10 mg/kg and 2.5 mg/kg on the left and center panels, respectively. $C_{int,p}$ represents the concentration of the released payload in the Ag+ cells. Fluctuations increase as β decreases. Furthermore, the time t_{max} corresponding to the maximum concentration C_{max} is gradually shifted to the right as β decreases and C_0 increases.

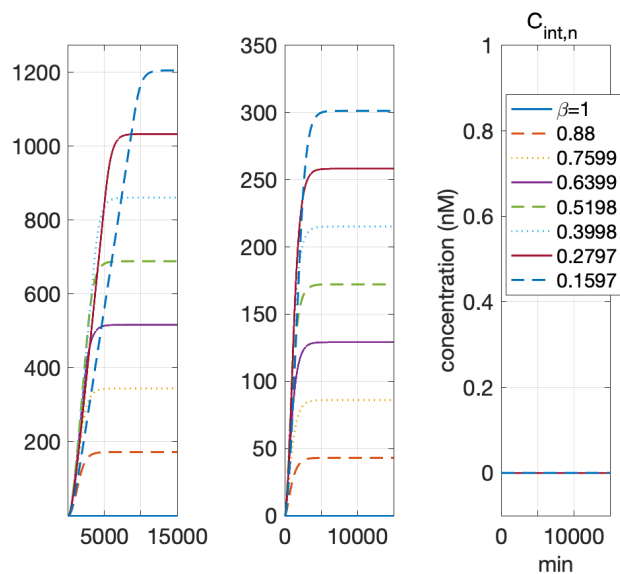


Figure 4. Control on the right panel and ADC administration of 10 mg/kg and 2.5 mg/kg on the left and center panels, respectively. $C_{int,n}$ represents the concentration of the released payload in the Ag- cells. This is related to the bystander-killing effect. The slope in the time phase during which the payload increases and the equilibrium points depend on the value of β .

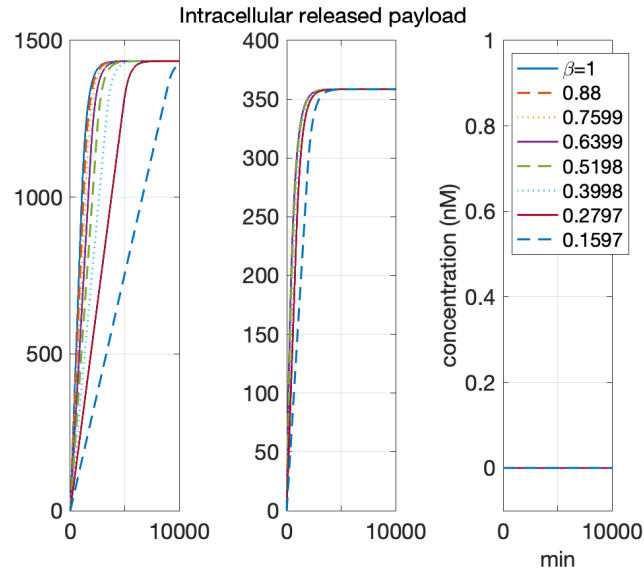


Figure 5. Control on the right panel and ADC administration of 10 mg/kg and 2.5 mg/kg on the left and center panel, respectively. The intracellularly released payloads are $C_{int,p} + C_{int,n}$. Equilibrium points are independent of β , but the slope in the time phase during which the payload increases depends on the value of β . In addition, this effect becomes more apparent as C_0 increases.

which is proportional to β . As the intracellular payload $C_{int,p} + C_{int,n}$ satisfies

$$(1 + k_{out})(C_{int,p} + C_{int,n}) = \alpha \cdot C_{int,adc} \cdot DAR + \frac{k_{in}}{\epsilon_p} C_{ext,p}.$$

This result appears to be unrelated to the Ag+ level because of the absence of β . However, as $C_{int,adc}$ depends on B_{adc} , which is equal to $\beta R_0 - \beta R$, the intracellular payload also depends on β ; however, this effect decreases as time passes because $C_{int,adc} \rightarrow 0$. As shown in the system (2.9), $C_{int,p} + C_{int,n}$ increases as β increases at time zero, and the effect of β is reduced as time passes until it becomes negligible. This result suggests that the ADC efficacy and bystander-killing are determined by the amount of intracellularly released payload rather than the Ag+ expression level, except in the time phase during which the payload increases. The ratio of

$$\frac{C_{int,p} + C_{int,n}}{(C_{int,p} + C_{int,n})|_{\beta=1}}$$

is plotted in Fig.8(a) and (b). As discussed, β and the target expression level influence the intracellular payload in the time phase during which the payload increases and then diminishes. In the next section, we investigate the influence of β on AUC.

3.4. Influence of β on AUC

In Fig.6(a), the ratio of the AUC of $C_{int,p}$ to $C_{int,p}|_{\beta=1}$ is plotted over β , and it is found that the AUC of $C_{int,p}$ and β are exactly proportional. This is independent of the initial value of the free ADCs. Fig.6(b) shows that the ratio of $C_{int,n}$ to

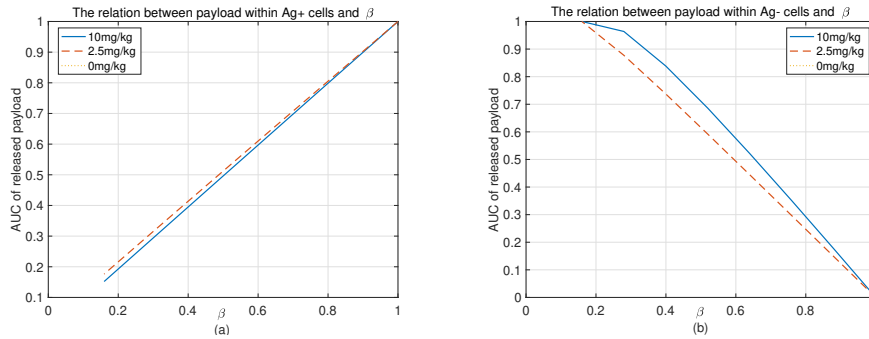


Figure 6. (a) AUC of the payloads over β profile within Ag+ cells. The relation is proportional to and independent of the amount of C_0 . The ratio is measured by $\frac{AUC_{c_{int,p}}}{AUC_{c_{int,p}|\beta=1}}$. (b) AUC of the payloads over β profile in Ag- cells. The relation is roughly inversely proportional, and C_0 has a lower influences on it. The shrinkage ratio is determined using $\frac{AUC_{c_{int,n}}}{AUC_{c_{int,n}|\beta=0.1597}}$.

$C_{int,n}|\beta=0.1597$ is inversely proportional to β . The ratio of the AUC of the released payload indicates that if C_0 is large, then the difference by β is larger, as shown in Fig.7. The smaller the initial administration, the smaller the influence of β . Thus, the intracellularly released payloads are influenced to a greater extent by the target-antigen expression levels at a higher concentration. It should be noted that the obtained results are slightly different from the results of Li et al. [19]. This is because we assumed the ratio of Ag- cells to Ag+ cells according to β with the fixed whole-cell; however, in the experiment conducted by Li et al., the type of payloads is the same, but the type of target antigen was specifically collected. This may result in different because the Ag+ target and the other target antigens are considered instead of the Ag+ target antigen and a different target antigen. Consequently, we may conclude that the larger the number of Ag+ cells under these conditions (i.e., no payload release before binding), the greater is the total payload accumulation in the intracellular space (Ag+/Ag- cells).

3.5. Bystander-killing effect and membrane permeability

The bystander-killing effect is related to $C_{int,n}$, the initial administration C_0 , and two parameters k_{in} and k_{out} , as shown in Fig.9. As the Ag+ expression levels increase, $C_{int,n}$ is expected to decrease, but it is uncertain from Eq.(2.8) owing to $C_{ext,p}$. However, as sufficient time passes,

$$C_{int,n} \rightarrow \frac{ca(1-\beta)}{a+1} = \frac{c(1-\beta) \cdot k_{in}}{k_{in} + k_{out}\epsilon_p},$$

where $a = k_{in}\epsilon_p^{-1}/k_{out}$. This indicates that $C_{int,n}$ increases as β decreases over time. k_{in} and k_{out} are parameters related to the membrane permeability, and the released payloads are required to have the ability to diffuse through the tumor for the bystander killing to occur. To explore the extent to which these parameters mediate the bystander killing, we considered k as k_{in}/k_{out} . We fix $k_{out} = 2.6266$ per min, as shown in Table 1 and give k a value greater than or equal to one to

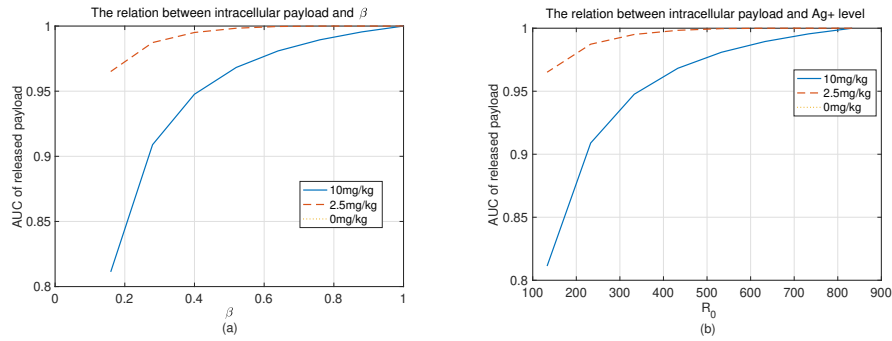


Figure 7. (a) Profile of the AUC of the payloads within intracellular space over β . The ratio is measured using $\frac{AUC_{c_{int,p}+c_{int,n}}}{AUC_{c_{int,p}+c_{int,n}|\beta=1}}$. (b) Profile of AUC over \tilde{R}_0 . The shrinkage ratio is determined as $\frac{AUC_{c_{int,p}+c_{int,n}}}{AUC_{c_{int,p}+c_{int,n}|\tilde{R}_0=833}}$. The greater the initial C_0 , the greater the shrinkage owing to the values of β and \tilde{R}_0 .

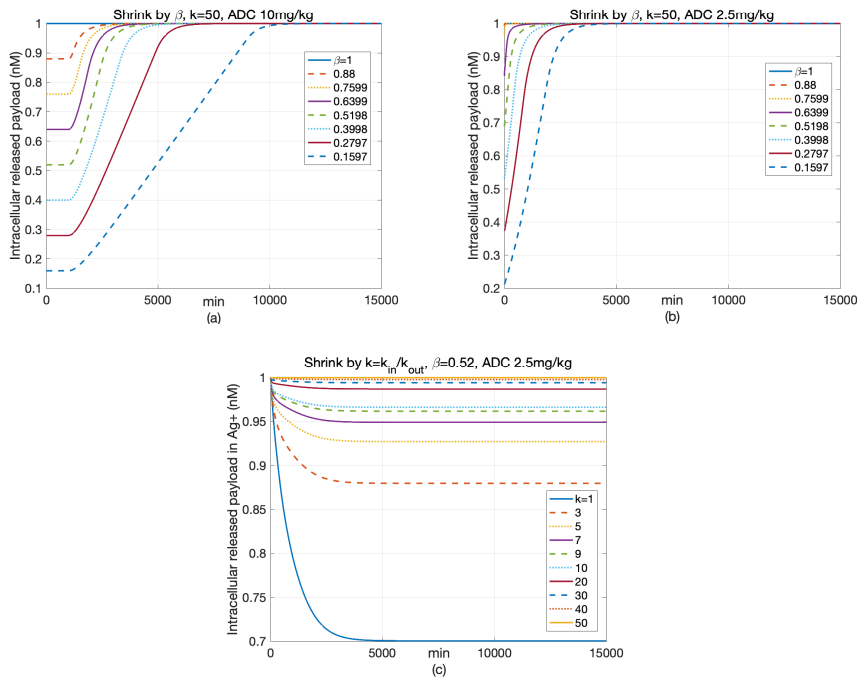


Figure 8. (a) Slope of the intracellular payloads depends on β , but the equilibrium points are independent of β . (b) If C_0 is small, then t_{max} is shifted to the right, and the change in the slope due to β is small. (c) $k = \text{influx/efflux}$ is investigated. From this and Fig.7(a), the influence of the change in k is predicted to be greater than that of β .

investigate the extent to which the permeability aids in determining the bystander killing effects. $1 \leq k \leq 50$ is assumed because $k \approx 50$, as described in [34]. The influence of k increases as k increases, as shown in Fig.9. As time passes, the loss of the intracellular payload is significantly decreased as k decreases. The model predicts that the effect of k is greater than that of β as shown in Figs. 8(b) and 7(b). This result supports the hypothesis that the membrane permeability is important for the bystander-killing effect, as shown in [19].

4. Discussion

The ADC mathematical model is developed for examining the influence of the change in Ag+/Ag- cells using $\beta \in (0, 1]$. The intracellularly released payloads $C_{int,p} + C_{int}$ depend on β in the time phase during which the payload increases, and the equilibrium points are independent of β . From the perspective of the AUC, the initial free ADC concentration determines the influence of β on the amount of intracellularly released payloads. The greater the value of β , the greater the AUC, but this may be difficult to capture if C_0 is small.

As β increases, the concentration of $C_{int,p}$ increases, the concentration of $C_{int,n}$ decreases, the AUC of $C_{int,p}$ increases linearly, and the AUC of $C_{int,n}$ decreases linearly. In summary, as β increases, the amount of the target antigen increases such that the free ADCs bind to a great extent, and the bounded ADCs are quickly delivered to $C_{int,adc}$. As a result, if β is not equal to one, then C_{max} and the equilibrium values over the time profile are different at $C_{int,p}$, and the smaller the value of β , the greater the relative difference. We also observed that C_{max} and the corresponding time t_{max} are shifted to the right as C_0 increases. Therefore, it is possible to predict the value of $C_{int,p}$ greater than expected if we do not consider the cells separately. If we consider a heterogeneous tumor environment as one homogenous type (i.e., $\beta = 1$), then a greater amount of payload in the Ag+ cells or intracellular space (Ag+/Ag- cells) may be predicted in the model than the actual amount. In addition, the intracellularly released payloads are affected by β to a greater extent at a higher C_0 , and the AUC exhibits a difference of approximately 20% for the approximate value of $10mg/kg$. As the concentration decreases, the effect of β decreases, and it is hardly noticeable at less than $2.5mg/kg$.

The bystander-killing effect is associated with $C_{int,n}$. The smaller the value of β , the greater the bystander killing. Furthermore, bystander killing is closely related to membrane permeability. The greater the value of k , the higher the concentration of both $C_{int,p}$ and $C_{int,n}$. This supports the experimental results obtained by Li et al. [19]. As β decreases, the equilibrium value of $C_{int,n}$ gradually increases, but the slope in the time phase during which the payload increases decreases. In particular, as shown in Fig.4, the smaller the value of β , the longer it takes to realize the same concentration. Moreover, the greater the value of C_0 , the greater the difference. This implies that the bystander killing could take a long time. Through in vivo experiments, we could determine to what extent the influence of β can be maintained via a measurement of the half-life of the cells if we estimate their degradation rate.

The advantage of this model is that the concentrations of $C_{int,p}$ and $C_{int,n}$ can be measured, such that it can be expected to decrease via the tumor growth inhibition (TGI) model. Moreover, the tumor reduction effect due to bystander killing may be confirmed using this model. Furthermore, as there is a delay in the increase of

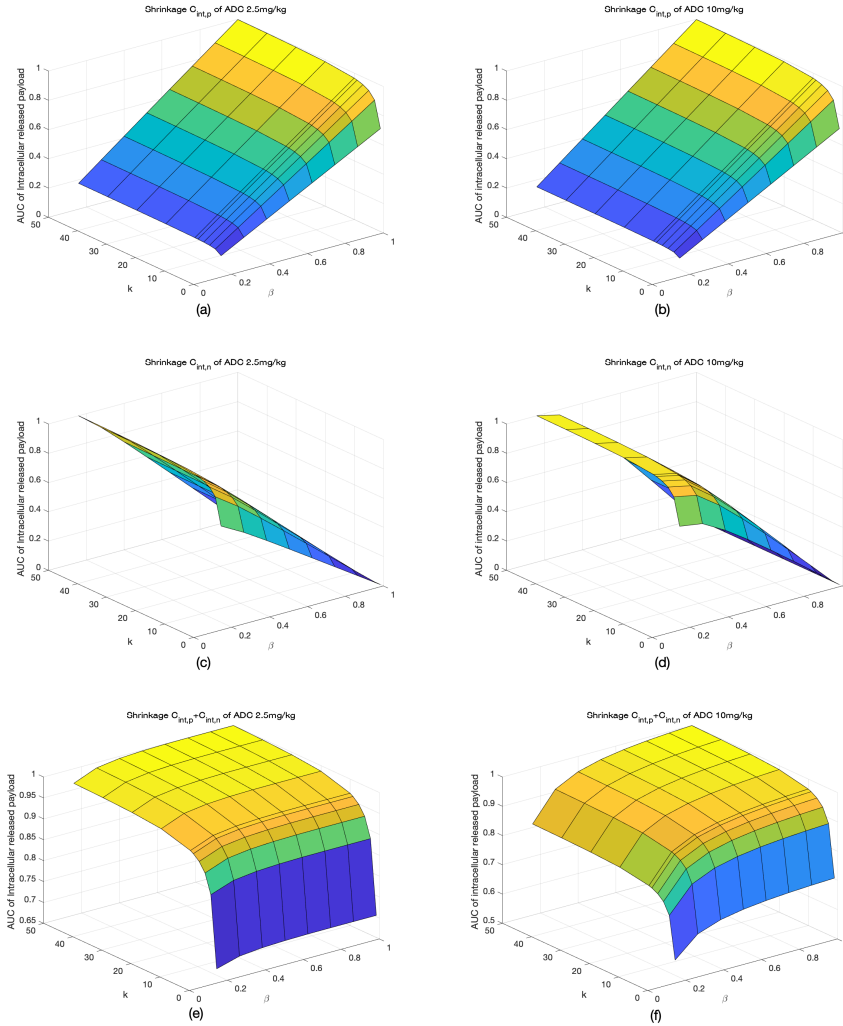


Figure 9. $k = k_{in}/k_{out}$. As k increases, the concentrations of $C_{int,p}$, $C_{int,n}$, and the intracellular payload increase. We perform a simulation to determine the relation between k , β , and AUC for two initial ADC concentrations. The impact of the permeability is crucial for the ADC efficacy related to the bystander killing as well as direct killing. As β increases, the intracellularly released payload is slightly increased, but this is hardly observed when the initial ADC concentration is low. (a) $\frac{C_{int,p}}{C_{int,p}|_{k=50,\beta=1}}$, $C_0 = 2.5mg/kg$. (b) $\frac{C_{int,p}}{C_{int,p}|_{k=50,\beta=1}}$, $C_0 = 10mg/kg$. (c) $\frac{C_{int,n}}{C_{int,n}|_{k=50,\beta=0}}$, $C_0 = 2.5mg/kg$. (d) $\frac{C_{int,n}}{C_{int,n}|_{k=50,\beta=0}}$, $C_0 = 10mg/kg$. (e) $\frac{C_{int,p}+C_{int,n}}{C_{int,p}+C_{int,n}|_{k=50,\beta=1}}$, $C_0 = 2.5mg/kg$. (f) $\frac{C_{int,p}+C_{int,n}}{C_{int,p}+C_{int,n}|_{k=50,\beta=1}}$, $C_0 = 10mg/kg$.

the payload concentration owing to β , it is possible to demonstrate a simpler model than the TGI model using the system with the Erlang distribution to capture it.

As shown in Fig.8(b) and (c), the amount of intracellularly released payload increases as β increases. However, an increase in the intracellularly released payload does not imply that the cell-killing effect is greater. This is because, even if the amount of the payload is greater than the threshold within a cell, it only kills that cell. Therefore, it is more efficient to distribute more than threshold rather than the payload quantity in a specific cell; however, it is difficult to capture such a phenomenon using our proposed model. There are several models that are suitable for this, especially the cylindrical Krogh model, which is used to determine the ADC penetration. Previous studies have described the limitations of the efficiency of the ADC owing to the binding site barrier and discuss that it is possible to modify the DAR or add mAbs to improve this efficiency. If those previous models are considered along with the target expression level, a more realistic prediction can be expected.

5. Conclusions

In this study, an ADC model was developed for extracting the intracellularly released payload. In this model, the payload clearance and tubulin binding processes are not taken into consideration for examining the impact of β and k on the intracellularly released payloads. As diffusion from the blood capillary to the tumor cells was not taken into consideration, the payload dynamics in the model were simple.

The dynamics of each compartment based on β or the target-antigen levels are predicted based on mathematical discussions, and the obtained results are verified via simulations. The effect of the membrane permeability on the intracellular payload concentration appears to be minimally influenced by the Ag+ expression levels. The ADC efficacy fairly supports the study of [4, 19] unless the value of C_0 is large.

The primary observations can be described as follows. The effect of the Ag+ expression levels is negligible, except in the time phase during which the payload increases. The parameters related to the membrane permeability, such as k_{in} and k_{out} , and its ratio k are investigated and are found to influence the intracellular payload concentration across all time phases. Li et al. [19] found via in vivo and in vitro experiments that the Ag+ expression levels may be less effective in reducing the bystander-killing effects; however, our model predicts that the effects of β are observed in the time phase during which the payload increases even for a small value of C_0 . The change in the AUC of the intracellular payload concentration is predicted up to approximately 20% according to the amount of C_0 .

There are fluctuations in the payloads in the Ag+ cells, which indicates that C_{max} and the equilibrium points do not coincide. As β and C_0 decrease, the fluctuations increase, and t_{max} is shifted to the right. Therefore, it is possible that the payload concentration is greatly predicted in the model if one does not consider dividing cells. To reduce the discrepancy between the results of the experiments and the models, we suggest that both the Ag+/Ag- cells obtained owing to the target expression levels be taken into consideration.

The model predicts that the higher the Ag+ level is, the shorter is the time to converge to the equilibrium points of the intracellular payloads. As C_0 increases, the influence of β also increases. The intracellular payloads converge to equilibrium points regardless of the value of k , and differences in the convergence time may be

correlated with the Ag+ target expression levels. The change in β is expected to significantly affect the number of intracellular payloads in the time phase during which the payload increases and this influence gradually disappears; however, the change in β is not expected to be greater than k .

A variety of phenomena can be evaluated using the proposed model. The model may present other findings reported in the literature [17,32] if the time phase during which the payload increases and in which the Ag+/Ag- cells are considered is emphasized. This model, while considering $C_{int,p}$ and $C_{int,n}$, could be applied to the tumor reduction model to mediate the bystander-killing effect.

We intend to develop a model for taking into consideration tumor penetration in the future. This model will take into consideration the binding rate, DAR, and cell type. It should be noted that it is assumed that the Ag+/Ag- cells are homogeneously mixed, and that there is some influence of β on the binding-site barrier.

Acknowledgment

This work was supported by the National Research Foundation of Korea (NRF) grant funded by the Korea government (MSIT) (NRF-2020R1C1C1A01004631 and NRF-2019R1A2C2007249).

References

- [1] P. J. Aston, G. Derks, B. M. Agoram and P. H. van der Graaf, *A mathematical analysis of rebound in a target-mediated drug disposition model: I. without feedback*, Journal of Mathematical Biology, 2014, 68(6), 1453–1478.
- [2] A. Beck, L. Goetsch, C. Dumontet and N. Corvaia, *Strategies and challenges for the next generation of antibody-drug conjugates*, Nature Reviews Drug Discovery, 2017, 16(5), 315–337.
- [3] A. Beck, T. Wurch, C. Bailly and N. Corvaia, *Strategies and challenges for the next generation of therapeutic antibodies*, Nature Reviews. Immunology, 2010, 10(5), 345.
- [4] E. R. Boghaert, K. Khandke, L. Sridharan et al., *Tumoricidal effect of calicheamicin immuno-conjugates using a passive targeting strategy*, International Journal of Oncology, 2006, 28(3), 675–684.
- [5] C. A. Boswell, D. B. Yadav, E. E. Mundo et al., *Biodistribution and efficacy of an anti-tenb2 antibody-drug conjugate in a patient-derived model of prostate cancer*, Oncotarget, 2019, 10(58), 6234.
- [6] J. H. Byun and I. H. Jung, *Modeling to capture bystander-killing effect by released payload in target positive tumor cells*, BMC Cancer, 2019, 19(1), 194.
- [7] R. V. Chari, *Targeted cancer therapy: conferring specificity to cytotoxic drugs*, Accounts of Chemical Research, 2007, 41(1), 98–107.
- [8] R. Deng, C. Zhou, D. Li et al., *Preclinical and translational pharmacokinetics of a novel thiomabTM antibody-antibiotic conjugate against staphylococcus aureus*, in *mAbs*, Taylor & Francis, 2019, 1–13.

- [9] H. P. Gerber, F. E. Koehn and R. T. Abraham, *The antibody-drug conjugate: an enabling modality for natural product-based cancer therapeutics*, Natural Product Reports, 2013, 30(5), 625–639.
- [10] L. Gibiansky and E. Gibiansky, *Target-mediated drug disposition model and its approximations for antibody–drug conjugates*, Journal of Pharmacokinetics and Pharmacodynamics, 2014, 41(1), 35–47.
- [11] C. P. Graff and K. D. Wittrup, *Theoretical analysis of antibody targeting of tumor spheroids: importance of dosage for penetration, and affinity for retention*, Cancer Research, 2003, 63(6), 1288–1296.
- [12] K. J. Hamblett, P. D. Senter, D. F. Chace et al., *Effects of drug loading on the antitumor activity of a monoclonal antibody drug conjugate*, Clinical Cancer Research, 2004, 10(20), 7063–7070.
- [13] N. Jain, S. W. Smith, S. Ghone and B. Tomczuk, *Current adc linker chemistry*, Pharmaceutical Research, 2015, 32(11), 3526–3540.
- [14] M. C. Janin-Bussat, M. Dillenbourg, N. Corvaia et al., *Characterization of antibody drug conjugate positional isomers at cysteine residues by peptide mapping lc–ms analysis*, Journal of Chromatography B, 2015, 981, 9–13.
- [15] J. Jin, G. Park, J. B. Park et al., *An anti-egfr \times cotinine bispecific antibody complexed with cotinine-conjugated duocarmycin inhibits growth of egfr-positive cancer cells with kras mutations*, Experimental & Molecular Medicine, 2018, 50(5), 67.
- [16] E. Khera, C. Cilliers, S. Bhatnagar and G. M. Thurber, *Computational transport analysis of antibody-drug conjugate bystander effects and payload tumoral distribution: implications for therapy*, Molecular Systems Design & Engineering, 2018, 3(1), 73–88.
- [17] Y. V. Kovtun, C. A. Audette, Y. Ye et al., *Antibody-drug conjugates designed to eradicate tumors with homogeneous and heterogeneous expression of the target antigen*, Cancer Research, 2006, 66(6), 3214–3221.
- [18] A. Krol, J. Maresca, M. W. Dewhirst and F. Yuan, *Available volume fraction of macromolecules in the extravascular space of a fibrosarcoma: implications for drug delivery*, Cancer Research, 1999, 59(16), 4136–4141.
- [19] F. Li, K. K. Emmerton, M. Jonas et al., *Intracellular Released Payload Influences Potency and Bystander-Killing Effects of Antibody-Drug Conjugates in Preclinical Models*, Cancer Research, 2016, 76(9), 2710–2719.
- [20] Q. Li, A. Barrett, B. Vijayakrishnan et al., *Improved inhibition of tumor growth by diabody-drug conjugates via half-life extension*, Bioconjugate Chemistry, 2019, 30(4), 1232–1243.
- [21] D. E. Mager and W. J. Jusko, *General pharmacokinetic model for drugs exhibiting target-mediated drug disposition*, Journal of Pharmacokinetics and Pharmacodynamics, 2001, 28(6), 507–532.
- [22] D. E. Mager and W. Krzyzanski, *Quasi-equilibrium pharmacokinetic model for drugs exhibiting target-mediated drug disposition*, Pharmaceutical Research, 2005, 22(10), 1589–1596.
- [23] R. K. Mittapalli, S. Stodtmann, A. Friedel et al., *An integrated population pharmacokinetic model versus individual models of depatuxizumab mafodotin*,

- an anti-egfr antibody drug conjugate, in patients with solid tumors likely to overexpress egfr*, *The Journal of Clinical Pharmacology*, 2019.
- [24] A. Mullard, *Maturing antibody–drug conjugate pipeline hits 30*, 2013.
- [25] N. M. Okeley, J. B. Miyamoto, X. Zhang et al., *Intracellular activation of sgn-35, a potent anti-cd30 antibody–drug conjugate*, *Clinical Cancer Research*, 2010, 16(3), 888–897.
- [26] H. L. Perez, P. M. Cardarelli, S. Deshpande et al., *Antibody–drug conjugates: current status and future directions*, *Drug Discovery Today*, 2014, 19(7), 869–881.
- [27] G. D. L. Phillips, G. Li, D. L. Dugger et al., *Targeting her2-positive breast cancer with trastuzumab-dm1, an antibody–cytotoxic drug conjugate*, *Cancer Research*, 2008, 68(22), 9280–9290.
- [28] L. Schwartz and I. de mathématique (Strasbourg), *Théorie des distributions*, 2, Hermann Paris, 1957.
- [29] A. P. Singh, L. Guo, A. Verma et al., *A cell-level systems pk-pd model to characterize in vivo efficacy of adcs*, *Pharmaceutics*, 2019, 11(2), 98.
- [30] A. P. Singh and D. K. Shah, *A “dual” cell-level systems pk-pd model to characterize the bystander effect of adc*, *Journal of Pharmaceutical Sciences*, 2019, 108(7), 2465–2475.
- [31] A. P. Singh, S. Sharma and D. K. Shah, *Quantitative characterization of in vitro bystander effect of antibody–drug conjugates*, *Journal of Pharmacokinetics and Pharmacodynamics*, 2016, 43(6), 567–582.
- [32] A. H. Staudacher and M. P. Brown, *Antibody drug conjugates and bystander killing: is antigen-dependent internalisation required?*, *British Journal of Cancer*, 2017, 117(12), 1736.
- [33] P. A. Trail, *Antibody drug conjugates as cancer therapeutics*, *Antibodies*, 2013, 2(1), 113–129.
- [34] C. Vasalou, G. Helmlinger and B. Gomes, *A mechanistic tumor penetration model to guide antibody drug conjugate design*, *Plos One*, 2015, 10(3), e0118977.
- [35] J. Wang, W. Shen and J. L. Zaro, *Antibody–Drug Conjugates: The 21st Century Magic Bullets for Cancer*, 17, Springer, 2015.
- [36] Wikipedia contributors, *Brentuximab vedotin — Wikipedia, the free encyclopedia*, 2018.
- [37] H. Yao, L. Feng, S. R. Suthe et al., *Therapeutic efficacy, pharmacokinetic profiles, and toxicological activities of humanized antibody–drug conjugate zt/g4-mmae targeting ron receptor tyrosine kinase for cancer therapy*, *Journal for Immunotherapy of Cancer*, 2019, 7(1), 75.